Impedance measurement and computation for the steam-generator tube integrity using the ECNDT technique

M. Chebout [1*], M. R. Mekideche [2], A. Hafaifa[1], A.Kouzou[1], H. Allag [2]

[1]*L2ADI Laboratory, Department of electrical engineering, Djelfa University, Algeria*
[2]*L2EI Laboratory, Department of electrical engineering, Jijel University, Algeria*
e-mail: chebout_med@yahoo.fr

Abstract. The purpose of this research paper is to characterize and extract crack defects from steam-generator (SG) tubes, operating in nuclear-power plants by using an eddy-current nondestructive testing (ECNDT) technique. Modeling and simulation using this technique make it possible to characterize the eddy-current sensors and to improve their performances while limiting the number of experimental prototypes and thus the development costs. The paper describes an effective ECNDT technique enabling detection of a small crack defect or discontinuity in the form of a narrow crack in cylindrical structures by using a particular sensor configuration based on the numerical technique. The results prove the efficiency of a 3D FEM model implemented based on the Comsol multiphysics software, which can understand , quantifies and accurately predicts the eddy-current signals determining the interaction between defected SG tube wall, and the eddy-current probe response. By using the multifrequency technique the entire crack depth of a conductive-test specimen is scanned. Our calculation results are verified by comparing them with the experimental ones and a good agreement between them is observed.

Keywords: Eddy current, Impedance, Nondestructive, Steam Generator, Sensor

Meritev in izračun impedance v ceveh parne turbine z uporabo tehnike ECNDT

V članku predstavljamo karakterizacijo napak v ceveh parne turbine v jedrskih elektrarnah na podlagi neporušnega testiranja z vrtinčnimi tokovi (ECNDT). S predlagano metodo lahko karakteriziramo senzorje vrtinčnih tokov. Predstavljena je učinkovita metoda ECNDT za odkrivanje manjših napak in razpok v valjnih strukturah z uporabo ustrezne konfiguracije senzorja. Rezultati potrjujejo učinkovitost modela 3D FEM, izdelanega s programsko opremo Comsol, ki lahko natančno oceni vrtinčne tokove in posledično ugotovi napake v strukturi. Rezultate merjenja smo analizirali z uporabo večfrekvenčne analize. Preverili smo dobljene rezultate in potrdili pravilnost predlaganega pristopa.

1 INTRODUCTION

The use of steam-generator (SG) units in the nuclear industry is extremely important for transferring the thermal energy and for separating the radioactive side of nuclear-power plants [1]. In nuclear-power reactors, heat is generated in the reactor core and transported through thousands of tubes within the steam generator as shown in Fig. 1. Irradiated primary-side water flows through the SG tubes at approximately 300°C [2] and heat is exchanged with the secondary side water whose temperature is increased to approximately 250°C [3].

The hot secondary-side water is converted into steam used to spin the turbines that generate electrical power using conventional electric generators. Thousands of thin-walled tubes provide an increased SG surface area necessary for an efficient heat transfer. The geometrical parameters such as the height, outer diameter and wall thickness of SG tubes are 7.5 m, 22.25 mm and finally 1.27 mm respectively. Detection of degradation in the SG tubes and components is important for maintaining the reactor efficiency and regular inspections are made [2].

In order to better assess SGs, it is desirable to identify their specific degradations, such as internal cracking, corrosion, high pressure and temperature, and characterize their extent which might lead to an industrial hazard catastrophe. Currently, regular inspections of SG tubes vary from plant to plant in terms of the frequency and percentage of the SG tubes to be inspected [3]. A common procedure in the United States for the light-water reactors is to inspect 20% of the total number of the SG tubes during each inspection cycle. Thus inspecting 100% of the SG tubes in five cycles [4].
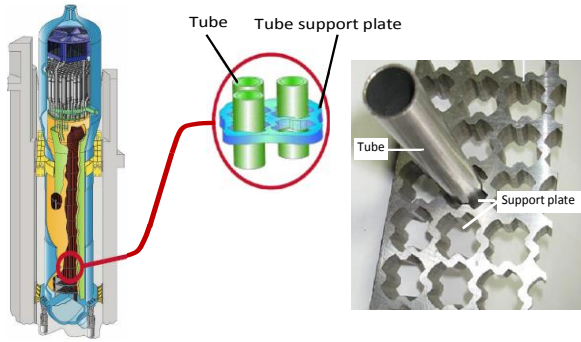
Figure 1. Steam generator cut away

To ensure the security of the entire installation, the SG operative is inspected in order to detect any possible defect or crack by using nondestructive testing (NDT) technique ensuring the installation uninterrupted operational and avoidance of any damage during testing [5].

Several nondestructive evaluation techniques are used [6]. In this paper, we review an ECNDT method that permits detection of a thin-size crack. Our approach is based on implementation of an efficient electromagnetic model for the evaluation of a millimetric crack defect submerged and buried on a three-dimensional cylindrical structure simulated as SG tube [7]. The paper also considers a probe-sensor scheme operated in an absolute and differential mode and validated by experimental results. Several authors treat a similar configuration mode [8], but the paper proposes a rather particular configuration of the probe coil enabling a faster and more efficient detection of crack-depth variations using a multifrequency technique approach and also enabling detection of simultaneous crack defects of various sizes and positions.

2 MATHEMATICAL MODEL

An eddy-current numerical modeling is set-up to analyze the eddy current testing phenomena and understand the interaction between the magnetic probe and crack defects. A multiple approaches based on an analytical technique and numerical analysis of a three-dimensional ECNDT is studied in [9] [10].

In this paper, a numerical approach based on FEM using a magnetic-vector potential and scalar-electric potential is used due to its flexibility and ability to handle complex structures containing thin-crack defects and taking into account anisotropic and inhomogeneous material properties [12].

The coil velocity is neglected and a quasi-static approximation is considered. Starting from the traditional $AV-A$ formulation:

$$\nabla \times \left(\mu^{-1} \nabla \times A \right) + \sigma \left(j\omega A + \nabla V \right) = J \quad (1)$$

$$\nabla \cdot \sigma \left(j\omega A + \nabla V \right) = 0 \quad (2)$$

Where $J = \sigma E$ represents the current density which depends on the tested material conductivity, $\omega = 2\pi f$ is the angular excitation frequency (rad/s) and $j = \sqrt{-1}$.

The integral of A-V formulation is obtained by applying the weighted residuals and the Galerkin's method for (1) and (2), using vector $\boldsymbol{\Psi}$ and scalar Ψ denoting the weighting functions which coincide with the shape functions in a finite-element realization [13]. Then (1) and (2) are replaced by:

$$\int_{\Gamma} \psi . \nabla \times \left(\mu^{-1} \nabla \times A \right) d\Gamma + \int_{\Gamma} \sigma \boldsymbol{\Psi} . \left(j\omega A + \nabla V \right) d\Gamma = \int_{\Gamma} \boldsymbol{\Psi} \cdot J \, d\Gamma \quad (3)$$

$$\int_{\Gamma} \psi . \nabla . \sigma \left(j\omega A + \nabla V \right) d\Gamma = 0 \quad (4)$$

Where Γ is the domain problem. Using the Gaussian theorem, (3) and (4) become:

$$\int_{\Gamma} \left(\frac{1}{\mu} \nabla \times \boldsymbol{\Psi} \right) \cdot \nabla \times A \, d\Gamma + \oint_{S} \boldsymbol{\Psi} \cdot \left(\frac{1}{\mu} \nabla \times A \times \boldsymbol{n} \right) dS + \int_{\Gamma} j\omega \sigma \boldsymbol{\Psi} \cdot A \, d\Gamma + \int_{\Gamma} \sigma \boldsymbol{\Psi} \cdot \nabla V \, d\Gamma = \int_{\Gamma} \boldsymbol{\Psi} \cdot J \, d\Gamma \quad (5)$$

$$\int_{\Gamma} \nabla \Psi . \sigma \left(j\omega A + \nabla V \right) d\Gamma - \oint_{S} \Psi \, \sigma \left(j\omega A + \nabla V \right) \cdot \boldsymbol{n} \, dS = 0 \quad (6)$$

where S is the surface which encloses Γ and $\boldsymbol{n}$ is the unit normal vector.

Finally, equations (5) and (6) can be rewritten as a function of the tangential component of the magnetic-field strength and the normal component of the current density [11]:

$$\int_{\Gamma} \left(\frac{1}{\mu} \nabla \times \boldsymbol{\Psi} \right) \cdot \nabla \times A \, d\Gamma + \oint_{S} \boldsymbol{\Psi} \cdot H_t \, dS + \int_{\Gamma} j\omega \sigma \boldsymbol{\Psi} \cdot A \, d\Gamma + \int_{\Gamma} \sigma \boldsymbol{\Psi} \cdot \nabla V \, d\Gamma = \int_{\Gamma} \boldsymbol{\Psi} \cdot J \, d\Gamma \quad (7)$$

$$\int_{\Gamma} \nabla \Psi . \sigma \left(j\omega A + \nabla V \right) d\Gamma - \oint_{S} \Psi \, J_n \, dS = 0 \quad (8)$$

The impedance calculation for the eddy-current inspection is very useful and interesting to understand and detect crack defects in SG tubes. The impedance expression of impedance is given as a function of excited current I and frequency f :

$$Z = R + j\omega L = \frac{1}{I^2} \left(P + j\omega W \right) \quad (9)$$

where P and W are the dissipated energy and the total stored energy, respectively , expressed by:

$$P = \int_{\Gamma} J \cdot E^* d\Gamma \quad \text{and} \quad W = \int_{\Gamma} H \cdot B^* d\Gamma \quad (10)$$

with $\boldsymbol{E} = -\nabla V - j\omega\boldsymbol{A}$, $\boldsymbol{B} = \nabla \times \boldsymbol{A}$ and $\boldsymbol{H} = \boldsymbol{B}/\mu$ (11)

where $\boldsymbol{E}$, $\boldsymbol{H}$ and $\boldsymbol{B}$ are the electric field, magnetic field and magnetic-flux density respectively

3. MEASUREMENT SETUP AND RESULTS

The goal is to get some information about the defects and to understand the physical phenomena in order to optimize the probe sensor and increase its capability to detect small defects by combining modelling and experimental techniques [14].

Figure 2 presents a three-dimensional model of a SG tube with the steel proprieties to be inspected.
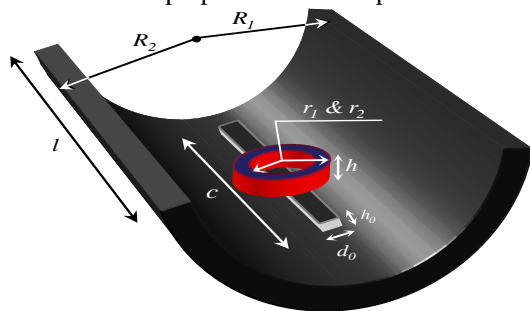
Figure 2. Geometrical model with a crack

The thickness of the specimen is $t = 2mm$, its inner diameter is $D_{Inn} = 10mm$, its height is $l = 40mm$, its conductivity is $\sigma_S = 1MS/m$, and its relative permeability is $\mu_r = 1$. A surface breaking crack appears in the middle of the cylindrical structure with dimensions: the width is $d_0 = 0.2mm$, the length is $c = 2\ mm$ of, and the depth is $h_0 = 0.12mm$ seen from internal surface of SG test specimen.

The coil of an absolute type is normally positioned on the surface of the tested structure with a constant *0.5mm* lift-off. Its axis is parallel to the z-axis of the coordinate system as shown in Fig. 2. The coil probe conductivity is set to $\sigma_{coil} = 56MS/m$ with the number of turns of $N=190$ used to drive the eddy-current and to detect the response. A multifrequency method is used employing a large excitation frequency interval ranging from some Hz to MHz in order to extract the defect signals.

A mesh with 413257 nodes and over 1.24 million of tetrahedral elements is adopted, providing a good approximation and yet tolerable computation times, especially with 200 μm of the crack width and 120 μm of crack depth. The modeling results of the SG tube are obtained by using a 3D model in the Comsol Multiphysics 3.5a software [15] and validated against the experimental results. Multiple benefits are ensured using this software because it allows simultaneous modelling of any combination of the three-dimensional phenomena, automatic mesh generation, equation solving, visualization and post-processing.

The eddy-current density is illustrated in Fig. 3. Its values are highly concentrated around the coil when the excitation frequency is 1.5 kHz.

Figs. 4 and 5 show an experimental and numerical calculation of the impedance component as a function of the coil displacement of crack occurrence.

The sensor position changes at a low pitch of 100 μm along or through a crack on an intern specimen surface. A pancake-type absolute by circular air-cored coil probe scans the SG structure surface and is parallel to the Z-axis.
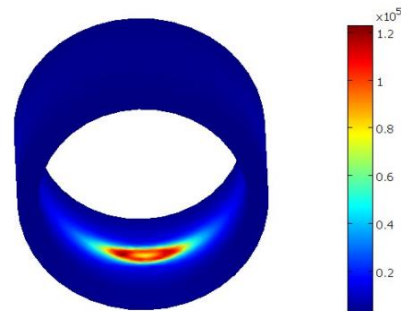

Figure 3. Induced eddy current density with no crack [A/m²]

The impedance components are determined by the energy and power calculations and interpreted based on changes in the resistance and reactance of the coil as explained by equations 9 and 10 [16]. The impedance-system is calculated at each position of the probe sensor. Two frequencies are selected; 150 kHz and 300 kHz to allow for a better understanding of the frequency effect on the eddy-current NDT operation. Our calculation and numerical results are compared with the experimental ones and a good agreement is observed.
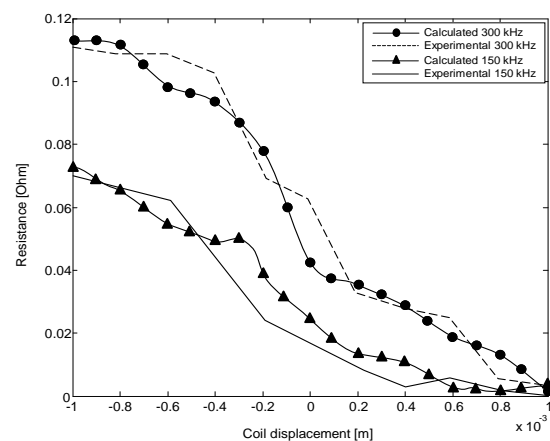

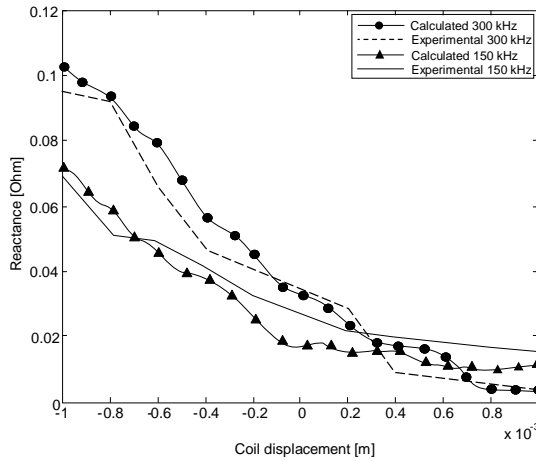Figure 4. Resistive-impedance components vs a coil displacement

Figure 5. Reactive-impedance components vs a coil displacement

The concept of normalized-impedance components given by the expression below is introduced [17]:

$$R_n = (R - R_0)/X_0 \qquad (12)$$

$$X_n = X/X_0 \qquad (13)$$

Were R_n and X_n are the normalized resistive component and the normalized reactive component respectively, Z_0 and Z are the impedance with no specimen test and the impedance of the conductive test material respectively.

An excellent overlapping between the experimental and numerical model results is observed on the normalized impedance plane shown in Fig. 6.
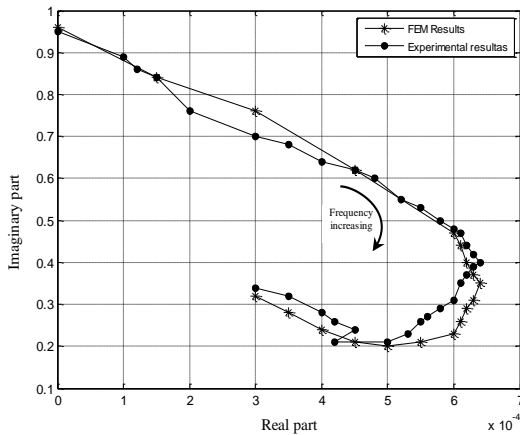

Figure 6. Normalized impedance plane diagram

When performing the above normalization, the measurement is not affected by the excitation coil (number of turns, no-load losses). It depends only on the SG tube parameters such as the excitation frequency, the probe geometry and target parameters. Namely, its geometry, electrical conductivity σ, magnetic permeability μ and lift-off distance are kept at 500 μm. Two probes made on a differential mode and spaced by a small distance of about 50 μm are considered and used to enable only local variations in the characteristics

of the product examined at a constant difference between two simultaneous measurements in two adjacent zones as shown in Fig. 7.
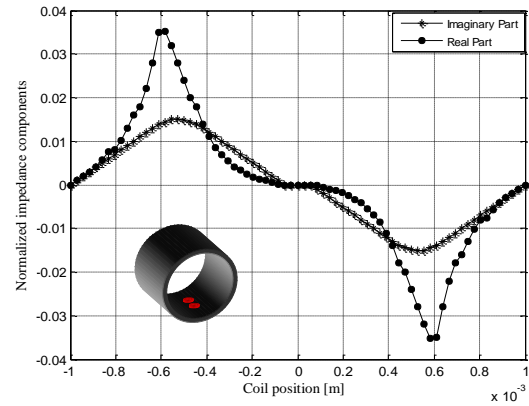

Figure 7. Normalized impedance components vs the coil position
This figure shows a variation in the real and imaginary part of the impedance for each displacement of the coil probe. The frequency excitation is 2 kHz and the lift-off distance is maintained at 500 μm. The imaginary component is much greater than the real component. Two phases are observed, the first one includes the phase where the defect is far away from the sensors giving a zero variation in the impedance. Once the first sensor detects a defect, the variation is visible and the two parts of the impedance increase to their maximal value. Then they become zero since the two coils see the same topography in order to be able to increase in the opposite direction and follow the same path as in the previous phase.
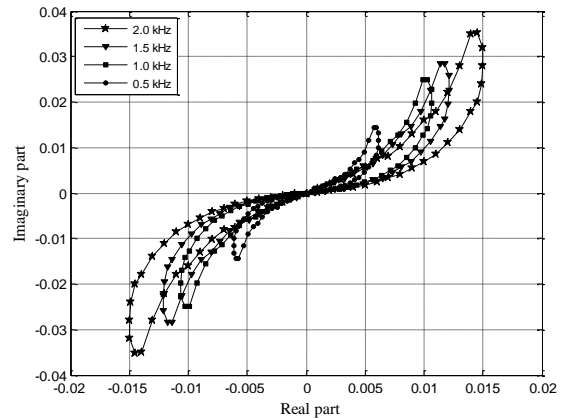

Figure 8. Frequency effect of on the impedance components

The impedance plane diagram is affected by the increase in the frequency value [18] as shown in Fig. 8. At low frequencies, the impact of variations in the thickness and lift-off on the normalized impedance is small due to the amplitude of the fields induced in the material. Similarly, at high frequencies, the impact of the SG tube on the normalized impedance components is limited due to the very small thickness of the skin which confirms the importance of excitation as a function of the variables to be quantified.

Fig. 9 illustrates two shapes and positions of a crack configuration in order to determine the change in the impedance-plane diagram of the cylindrical structure.
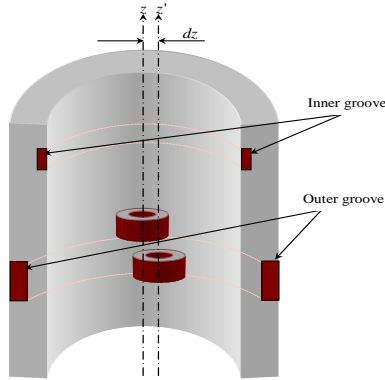

Figure 9. Crack shape and location in a perpendicular mode

In Fig. 10, the variation in the impedance components is greater when the crack is in the outer position than in the inner position. Also to be noted that the shape of the impedance-plane trajectory changes with the position of the crack defect in the support plate tube. The eccentricity of the probe is also considered when its scans the cylindrical structure. Here, eccentricity distance dz is between -0.1 mm and 0.1mm.
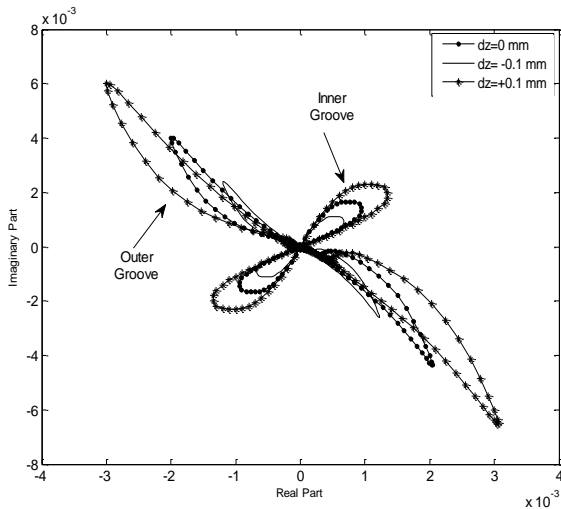

Figure 10. Probe eccentricity effect on the impedance plane

To evaluate the limits of the flaw detection [19], the ΔR_n and ΔX_n notions are considered.

$$\Delta R_n = R_n\left(Unflawed\right) - R_n\left(flawed\right) \qquad (14)$$

$$\Delta X_n = X_n\left(Unflawed\right) - X_n\left(flawed\right) \qquad (15)$$

The variation in the normalized impedance components is plotted for three values of crack depth: 0.3 mm, 0.6 mm and at 0.9 mm from the cylindrical tube surface shown in Figs. 11 and 12. They describe the variation in the real and imaginary part of the normalized impedance as a difference between the case with and with no crack.
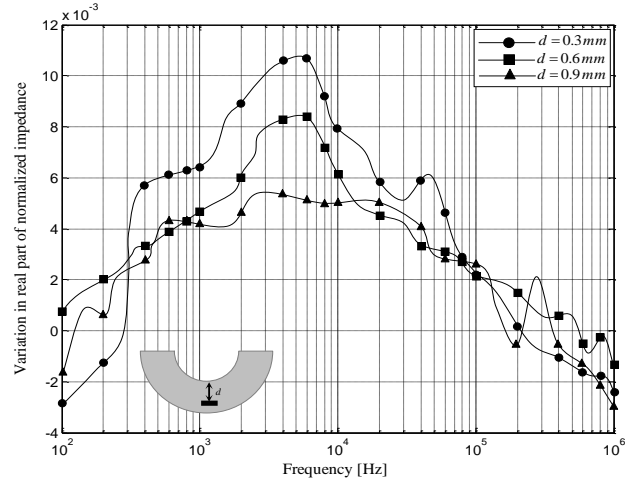

Figure 11. ΔR_n vs the frequency for different crack depths

There is a difference noted between the two figures. The variation in the resistive part is slightly higher than the variation in the inductive part and the frequency values at which the variation is the highest vary from one component to another. It is shown that the deeper the crack is, the smaller is the variation in the two impedance components meaning that the chances to detect it are scarce.
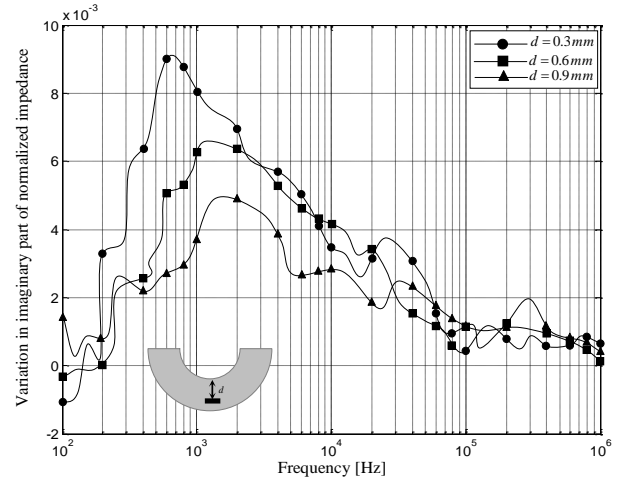

Figure 12. ΔX_n vs the frequency for different crack depths

4. CONCLUSION

The paper proposes an efficient technique for evaluating the interaction between the electromagnetic field of an absolute and differential probe mode and a metallic tube in order to predict the presence of a 3D planar crack defect. Comparing the numerical results with the laboratory-based measurement data shows a good agreement. The impact of various frequencies and crack parameters on the signal response is investigated and the results show that using the solution with three dimensional finite elements enables prediction and evaluation of the characteristic response of the eddy-current probe to crack defects in SG tubes. The further

work will be forwards reconstruction of crack shapes by using enabling detection of crack profiles from simulated eddy-current testing-response signals that will be experimentally verified.

REFERENCES

[1] H.S.Shim, M.S.Choi, D.H.Lee and D.H.Hur, "A prediction method for the general corrosion behavior of Alloy 690 steam generator tube using eddy current testing", *Nuclear Engineering and Design,* 297, 26–31, 2016.

[2] S. Girard,T.Romary,J.M.Favennec,P. Stabat and H. Wackernagel, "Sensitivity analysis and dimension reduction of a steam generator model for clogging diagnosis", *Reliability Engineering and System Safety*, 113, 143–153, 2013.

[3] D.H.Hur, M.S. Choi, H.S. Shim, D.H. Lee and O. Yoo, "Influence of signal-to-noise ratio on eddy current signals of cracks in steam generator tubes", *Nuclear Engineering and Technology*, 46, n 6 883–888, 2014.

[4] M.Jesenik, M.Beković, A. Hamler and M. Trlep "Searching for hidden cracks and estimations of their depths by using the database", *NDT&E International*, 86, 44–52, 2017.

[5] J.A.Buck, P.R. Underhill, J.Morelli and T.W Krause, "Simultaneous multiparameter measurement in pulsed eddy current steam generator data using artificial neural networks", *IEEE Transactions On Instrumentation And Measurement*, 65, n 6, 672–679, 2016.

[6] C. Hellier, "Handbook of Nondestructive Evaluation", McGraw-Hill Education, 2nd edn. 2012.

[7] A.Rosell, "Efficient finite element modelling of eddy current probability of detection with transmitter–receiver sensors", *NDT&E International*, 75, 48–56,2015.

[8] H.Zaidi, L.Santandréa, G.Krebs, Y.Le Bihan and E.Demaldent, "Modeling of thin conducting and magnetic Layers in eddy current testing by overlapping finite elements", *COMPEL*, 39 n 1-4, 341–346, 2012.

[9] J.García-Martín, J.Gómez-Gil, E.Vázquez-Sánchez, "Nondestructive techniques based on eddy current testing", *Sensors*, 11 n3, 2525-2565, 2011.

[10] J.R.Bowler, T.P.Theodoulidis, H. Xie and Y. Ji, "Evaluation of eddy current probe signals due to cracks in fastener holes", *IEEE Transactions on Magnetics*, 48, n3,1159–1170,2012.

[11] M.Augustyniak and Z.Usarek, "Finite Element Method Applied in Electromagnetic NDTE: A Review" *Journal of Nondestructive Evaluation*, 35, n3, 35–39,2016.

[12] G.Sposito, P. Cawley and P.B.Nagy,"An approximate model for three-dimensional alternating current potential drop analyses using a commercial finite element code", *NDT & E International*, 43 n2,134-140,2010.

[13] R.Hamia, C.Cordier and C.Dolabdjian, " Eddy current nondestructive testing system for the determination of crack orientation", *NDT & E International,* 61, 24–28,2014.

[14] S.Bennoud,M.Zergoug and A.Allali, "Numerical simulation for crack detection using the finite element method", *The International Journal of Multiphysics*,8 n1,1–10,2014.

[15] L.Santandréa and Y.Le Bihan, " Using COMSOL Multiphysics in an eddy current nondestructive testing context", *Proceeding of the COMSOL Conference*, Paris, France, 2010.

[16] L.S.Rosado, T. G.Santos, P. M.Ramos, P.Vilaça and M.Piedade, "A differential planar eddy-currents probe: fundamentals, modeling and experimental evaluation," *NDT and E International*, 51, 85–93, 2012.

[17] L.S.Rosado, J. C. Gonzalez, T. G.Santos, P. M.Ramos and M.Piedade, "Geometric optimization of a differential planar eddy-currents probe for non-destructive testing" , *Sensors and Actuators A Physical*, 197, 96–105, 2013.

[18] H.Lemire, P. Underhill, T. Krause, M. Bunn and D. Butcher "Improving probability of detection of bolt hole eddy current inspection", *Research in Nondestructive Evaluation*, 21 n3, 141–156,2010.

[19] W. Cheng, "Thickness Measurement of Metal Plates Using Swept Frequency Eddy-Current Testing and Impedance Normalization", *IEEE Sensors Journal*, 17 n14, 4558 - 4569, 2017.

Mohammed Chebout received his engineer degree in electrical engineering from the University of Jijel in 2003. From December 2008 he has been a researcher and an assistant professor at the Djelfa University. He is a member of a research team of the L2ADI Laboratory, where he is forward his PhD degree on finding new algorithms and optimization methods for the diagnosis and identification of crack forms based on different NDT techniques.

Mohamed Rachid Mekideche received his diploma in electrical engineering from the USTO University at Oran, Algeria. In 1981, he joined the National Polytechnic School of Algiers as an assistant and post-graduate student preparing his master degree thesis. After receiving his PhD, degree from the University of Nantes (France) he became professor. He is now with the University of Jijel where he is a teacher and Dean of the Engineering faculty. He is the author and co-author of many works published or presented at international conferences.

Ahmed Hafaifa received his state engineer degree in 2000 in Applied Automation and the M.SC and PhD degrees on Applied Automation and Signal Processing in 2004 and 2010 respectively from the UMBB Boumerdes University. He is a full Professor teaching in Industrial Processes: Automation / Diagnosis and Reliability Engineering at the Science and Technology Faculty of the University of Djelfa, Algeria. Currently he is a Director of the L2ADI Laboratory of the University of Djelfa.

Abdellah Kouzou received his State Engineering degree, the M.SC and PhD degrees from the University of Tiaret, Algeria, University of Boumerdes, and Polytechnics Superior National School respectively. Since 2010, he has been a researcher with technical university of Munich in Germany and is a collaborating researcher with the Texas A&M University at Qatar.

Hicham Allag received his engineering degree in electrical engineering from the University of Jijel, Algeria, in 2001, and his M.Tech. and Ph.D. degrees in electrical engineering from the Mentori University of Constantine and Grenoble Institute of Technology in 2005 and 2009 respectively. Since 2009, he has been with the department of electrical engineering, University of Jijel, where he is currently Professor in 2017. His research interests are in Permanent-Magnet measurement, analytical calculation of magnetic field, forces, energy in Permanent- magnet systems, superconductivity systems, nondestructive testing and evaluation.